Hindawi
International Journal of Photoenergy
Volume 2022, Article ID 8799060, 11 pages
https://doi.org/10.1155/2022/8799060

Research Article

Full Silicon Tandem Solar Cells Based on Vertically Aligned Nanostructures

Dmitry A. Kudryashov,[1,2] **Ivan A. Morozov**,[1,2] **and Alexander S. Gudovskikh**[1,2]

[1]*Photonic Department, Saint-Petersburg Electrotechnical University "LETI", Saint-Petersburg 197376, Russia*
[2]*Renewable Energy Laboratory, Alferov University, Saint-Petersburg 194021, Russia*

Correspondence should be addressed to Alexander S. Gudovskikh; gudovskikh@spbau.ru

Received 27 September 2021; Accepted 3 February 2022; Published 28 February 2022

Academic Editor: P. Davide Cozzoli

A three-dimensional computer simulation of flexible double-junction solar cells (SC) consisting of Si wires and p-i-n a-Si:H structures was carried out. The performance dependence on geometrical and electrical parameters was calculated. With an increase in the height of the Si wires, the open-circuit voltage (V_{OC}) decreases monotonically for both the bottom Si and the top p-i-n a-Si:H junctions. The short-circuit current density (J_{SC}) for the top p-i-n a-Si:H junction increases sharply with Si wire height, and then, it goes into saturation at a wire height of more than 10-15 μm. The absolute value of J_{SC} increases (from 10.2 to 12.7 mA/cm^2) with a decrease in the wire diameter (from 2 to 0.5 μm). For the bottom junction based on Si wires, the dependence of J_{SC} on the wire height is determined by the charge carrier lifetime, doping level, and diameter, which can be associated with the effect of complete inversion of the Si wire conductivity type. For tandem SCs, the optimal wire height is 10 μm, at which efficiency of 14% can be achieved for structures based on Si wires with a diameter of 0.5 μm and a charge carrier lifetime of 10 μs. The practical implication of the developed design was experimentally demonstrated.

1. Introduction

The upcoming energy engineering is projected to rely heavily on renewable energy sources such as wind and solar power. By now, for example, in Germany [1], the share of electricity production from renewable energy sources accounts for about 47.9% of all energy sources. The number of solar panels installed in households and converting sunlight into heat or electricity is getting more from year to year worldwide. A large number of portable devices supplied with solar cells (SC) have started to appear in the market, but SC efficiency is still low. Namely, the highest efficiency achieved for the single-crystal silicon-based SC is currently 26.7% [2], and this indicator is almost very close to the theoretical limit of 30% [3]. By replacing silicon, as an active region, with gallium arsenide, it is possible to raise this indicator up to 29.1% [2]. However, the use of silicon only or compounds of the III-V type as a base does not ensure converting the entire spectrum of solar radiation, because the photons with energies less than the bandgap (E_g) of the active region material do not participate in the generation of the electron-hole pairs. On the other hand, the photons with energies higher than E_g heat the semiconductor due to light-generated charge carrier thermalization. The solution to this problem was the approach in which the solar cell includes several active regions—semiconductors with different values of E_g, arranged in decreasing order. Such solar cells are called multijunction solar cells. So, the efficiency for a five-junction solar cell has achieved 38.8% [2] for AM1.5G one sun conditions.

To effectively compete with traditional energy sources such as gas and oil, solar cells, in addition to high efficiency, must have a low cost, be environmentally friendly, and also have stable characteristics, despite sometimes extremely hard temperature conditions.

So-called flexible electronics are getting more and more promising there where the design of the device tends to bend within certain permissible limits while maintaining its performance. For example, a flexible solar cell could cover the

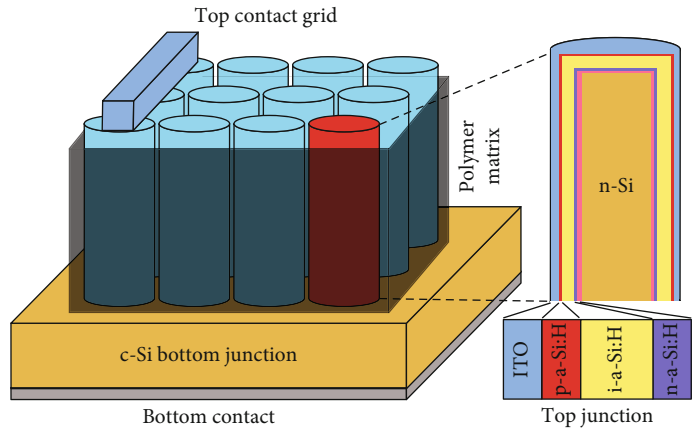

Figure 1: Schematic representation of a nanowire-based solar cell.

surface of a balloon and drive an engine giving it an almost unlimited flight time. Unused car roof surfaces could also generate additional energy with a flexible solar panel.

The problem is that semiconductor compounds are often quite fragile materials. Bending resistance can be increased by making a substrate thinner [4]. Moreover, in this case, the recombination losses for silicon are reduced, which makes it possible to use silicon with a lower carrier lifetime. However, it is useless to make the silicon substrate too thin because of weak light absorption in silicon.

There are some materials with a higher absorption coefficient than silicon. For example, in perovskites SC, the active region thickness does not exceed a micron, while the efficiency of such cells by now has reached 22.6% [2], and in the silicon/perovskite tandem—29.5% [2]. At the same time, perovskite SCs have not demonstrated yet the level of stability inherent in traditional SCs [5].

Flexible thin-film SCs based on amorphous hydrogenated silicon are also widespread, although their efficiency for the case of a single-junction SC has not exceeded 10% [2].

So, there is a problem of searching for materials and structures for manufacturing a highly efficient flexible SC. There is also a key question: in modern SCs, up to 50% of the cost is a substrate price, and if it is possible to replace the substrate with something less expensive or reduce its consumption, then such SCs would find their niche in the market.

To create a flexible SC, one can use a thin substrate made of a semiconductor, which is at the same time an active region of the SC. However, even in the case of silicon, the cost of manufacturing such substrates would be extremely high, and a lot of material might be lost during its manufacture (grinding, polishing, and etching).

The material of the active region of the SC can be applied to an already existing polymer substrate. Such a substrate should have high-temperature stability, good adhesion, and high strength. So, for example, on substrates based on polyimide, prototypes of solar cells based on CdTe or a-Si:H were made [6, 7]. However, it should be noted that due to the different coefficients of thermal expansion of the substrate materials and the deposited layers, mechanical stresses arise, which can subsequently lead the SC to degradation.

The problem can be solved by combining the above approaches taking into account the fact that nanoscale silicon structures would act instead of a thinned silicon substrate, and a polymer matrix would be used to hold them (Figure 1). In this case, the polymer is to provide strength and flexibility to the entire structure, and the silicon nanostructures would not deform during bending.

The nanosized silicon structures are supposed to be a tandem (two junctions) SC made in a core-shell design. The bottom junction would be made based on multi- or monocrystalline silicon covered with a wide-gap passivating layer (a-Si:H). Next would be the tunnel junction or transparent conductive layer for electrical connection between the top and bottom junctions. The top p-i-n junction is based on a-Si:H. Thus, most of the *i*-layer of the top junction would be located perpendicular to the surface of the substrate. In these vertical regions, the absorption of solar radiation would be much higher due to the greater length of the structure (5-10 μm) than in the planar version. Thus, high optical absorption could be achieved with a low thickness of the *i*-layer. An increase in the effective optical thickness of the top junction while maintaining a high electric field strength due to the small thickness makes it possible to achieve higher values of the short circuit current density (J_{SC}) of the top junction, which has been demonstrated experimentally [8]. The increase in short-circuit current is necessary to match the current with the bottom c-Si junction since J_{SC} is strongly limited for a planar a-Si:H p-i-n junction.

However, to achieve results of practical interest, it is still necessary to solve several fundamental problems associated, for example, with an assessment of the maximum achievable efficiency of such photovoltaic structures, which is a rather difficult task, and therefore, in the literature, there are only solutions to particular problems and not the general picture (tandem SC). For example, in [9], the FDTD method was used to simulate the optimal height of a single-junction core-shell SC, which was about 2 μm. The reflection from such a structure at a column diameter of 60–160 nm was about 0.3%, which was subsequently confirmed experimentally.

In general, quite a lot of the papers were devoted to modeling reflection from columnar structures determining

Table 1: Parameters of the layers of the tandem a-Si:H/c-Si SC.

Material	E_g (eV)	Thickness (μm)	Doping level (cm $^{-3}$)	Fermi level position (eV)	Electron affinity (eV)
(p) a-SiC:H	1.9	0.01		0.4	3.8
(i) a-Si:H	1.72	0.2		0.85	3.9
(n) a-Si:H	1.72	0.03		0.3	3.9
Tunnel diode					
(p) a-Si:H	1.72	0.02		0.4	3.9
(n) c-Si (wire)	1.12	Diameter 0.5–2; height 2–30	10^{15}-10^{17}	0.1-0.28	4.05
(n) a-Si:H	1.72	0.02		0.3	3.9

the optimal height, diameter, and period [10]; however, a complex solution that takes into account the electrophysical phenomena occurring inside the light converting structure requires serious study.

In [11], using 3D modeling, the structure of c-Si/a-Si/AZO/glass in a core-shell design was investigated to reveal the degree of influence of surface recombination at various interfaces of the structure on the SC electrical characteristics. It was shown that for a structure with a height of 10 μm and a ratio of the column diameter to the period equal to 0.8, the calculated value of the efficiency was 13.95%.

In [12], a comprehensive calculation of a core-shell structure for a tandem SC based on III-V nanowires on silicon was carried out. Materials such as InP, GaAs, AlGaAs, and GaInP were considered. A comparison was made between the radial junction and axial junction configurations. It was demonstrated that the radial junction variant is more resistant to surface recombination than the axial junction. It was shown that for a solar cell composed of a silicon-based bottom junction and an $Al_{0.2}Ga_{0.8}As$ top junction material with a column height of 10 μm, the maximum possible theoretical efficiency was 40%.

In [13], the properties of a silicon radial solar cell consisting of a p-type silicon core with a radius of 80 nm covered with a 20 nm layer of undoped silicon and then 20 nm n-Si were modeled. Calculations showed an efficiency of 8.2%. The optimal value of the efficiency was achieved with a column length equal to the diffusion length of minority charge carriers and doping of the order of 10^{18} cm^{-3}.

In [14], a similar radial structure was simulated, but it was demonstrated that a single-junction SC can show efficiency of up to 12%. At the same time, the n-core nanowire structure had better characteristics in comparison with the p-core nanowire structure and the standard 1D structure. It was also shown that the length of the nanowire was not a governing parameter.

Thus, the purpose of this study is to calculate the performance of a tandem SC fabricated using vertically aligned nanostructures.

2. Methods

The simulation was carried out using the Silvaco ATLAS software, which uses finite element discretization to define the geometry of the device and determine the elements and nodes, for which the physical properties can be calculated [15, 16]. This program performs a numerical solution of the continuity equation and Poisson equations for each layer using different boundary conditions and external influences (applied stress, lighting). A band diagram, the main characteristics of solar cells (SC), and various electrical measurements allowing analyzing the results of experiments can be simulated. The modeling reasonably predicts the properties of heterostructures of various designs when the actual parameters of the layers and interfaces obtained from the previously mentioned characterization methods are introduced. This approach provides recommendations for optimizing the design of multijunction SC.

Due to the program limitations, it was not possible to calculate the entire tandem SC in 3D mode; therefore, to evaluate the operation of the tandem SC, the top and bottom junctions were calculated separately, and then, the current and voltage were matched to calculate the I–V curves of the tandem SC. In the developed model, the top and bottom contacts were considered ohmic. To estimate the maximum achievable values of the solar energy conversion efficiency, the reflection coefficient from the front surface of the solar cell was set equal to zero. Absorption spectra were taken from literature data.

A common weakness in computer simulations is that the calculation accuracy is determined by property completeness description for the materials used in the calculations. Thus, the parameters of the a-Si:H layers are determined in the study of SC based on a-Si:H p-i-n structures fabricated by the Oerlikon technology at the R&D Center for Thin-Film Technologies in Energetics of Hevel Solar company [17], the main of which are presented in Table 1. This structure performance is well known. It acts as the top junction in the considered tandem SC. The results of calculations of its energy band diagram and density of states are shown in Figure 2. The calculated I–V curves coincided with sufficient accuracy with the measured experimental values.

Figure 3 shows a three-dimensional model of a single tandem SC used in the calculations. In the calculations, the diameter of the silicon wire was varied from 0.5 to 2 μm. To assess the influence of the quality of silicon on the performance of the SC, we used two extreme values, the lifetime of minority charge carrier (MCC) in silicon, 10 μs and 1 ms. Solar radiation with an intensity of 100 mW/cm^2 and an AM1.5 spectrum fell vertically.

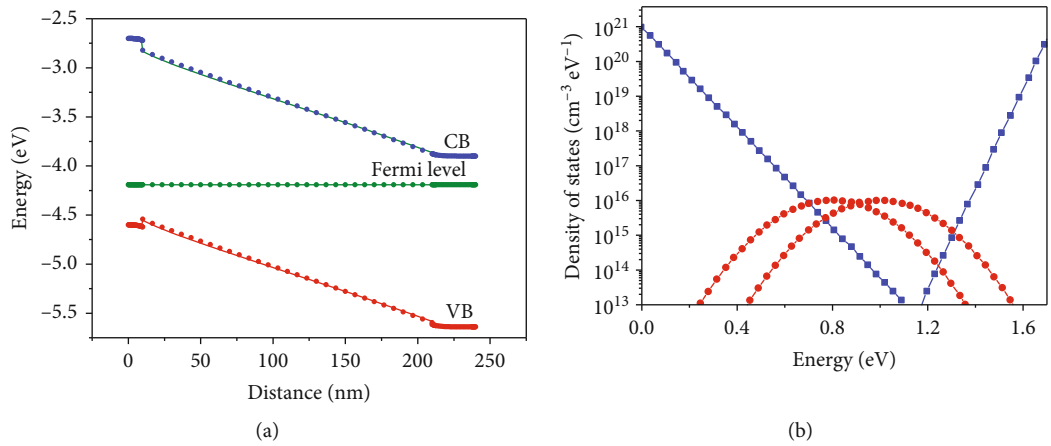

Figure 2: (a) Calculated equilibrium band diagram of the top p-i-n junction and (b) distribution of states in the gap of a-Si:H.

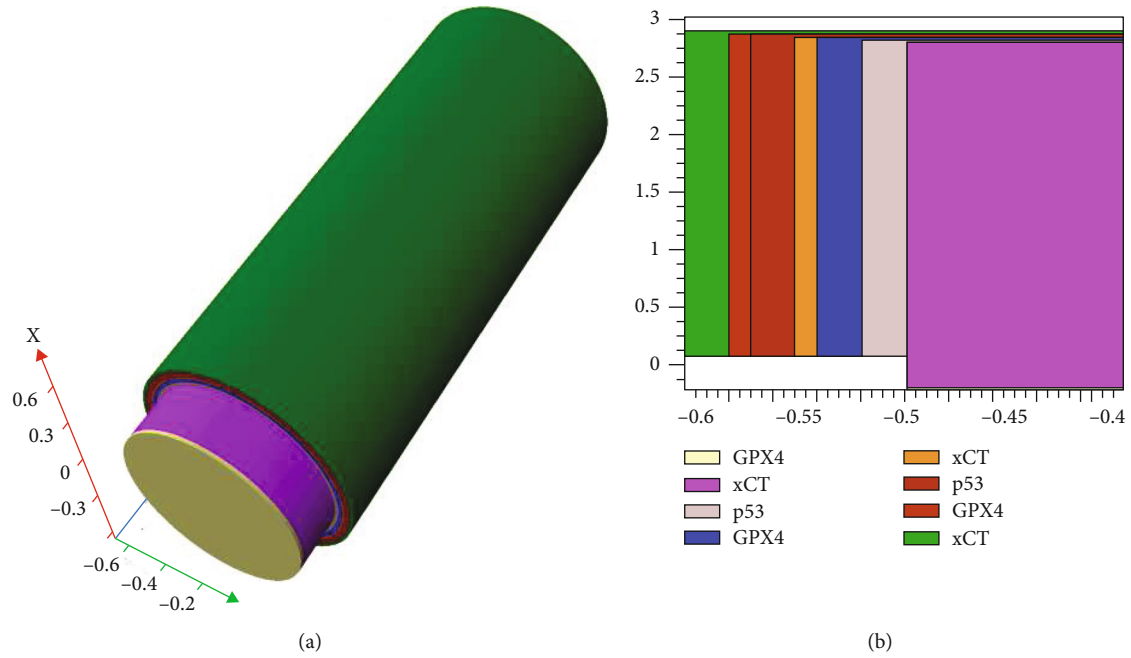

Figure 3: Graphic representation of the three-dimensional model of the solar cell (a) and an enlarged section of the wall side (b).

3. Results and Discussion

3.1. Bottom Junction. The calculation of the bottom junction performance has shown that in the case of high values of MCC lifetime (1 ms) an increase in the height of the silicon wire is accompanied by a significant increase in the short-circuit current density (J_{SC}) and a slight decrease in the open-circuit voltage (V_{OC}) (Figure 4). An increase in J_{SC} is associated with an increase in the number of absorbed photons and, therefore, of generated electron-hole pairs. A slight decrease in V_{OC} is caused by the recombination losses, which rise with increasing the distance that must be overcome by the charge carriers due to diffusion. The obtained dependence has the same behavior for all diameters of Si wires and doping levels, which are in the range of 0.5–2 μm and 10^{15}-10^{17} cm^{-3}, respectively.

If the obtained dependencies for the high value of the MCC lifetime are predictable, then the dependencies for the small value of the MCC lifetime are more complex (Figure 5). For the Si wire diameter of 0.5 μm, J_{SC} does not depend on doping and increases monotonically with an increase in the wire height to 10 μm. For higher wire height (>10 μm), the behavior of J_{SC} depends on the doping level: for 10^{17} cm^{-3}, the increase is going on, and for 10^{16} cm^{-3}, the increase is getting weaker, while a decline is being observed for 10^{15} cm^{-3}. For larger wire diameters, J_{SC} increases monotonically with increasing Si wire height regardless of the doping level. V_{OC} decreases monotonically with increasing Si wire height, but the absolute value of V_{OC} depends on the doping level.

The observed behavior is associated with the fact that at a small diameter of the Si wire and a low doping concentration,

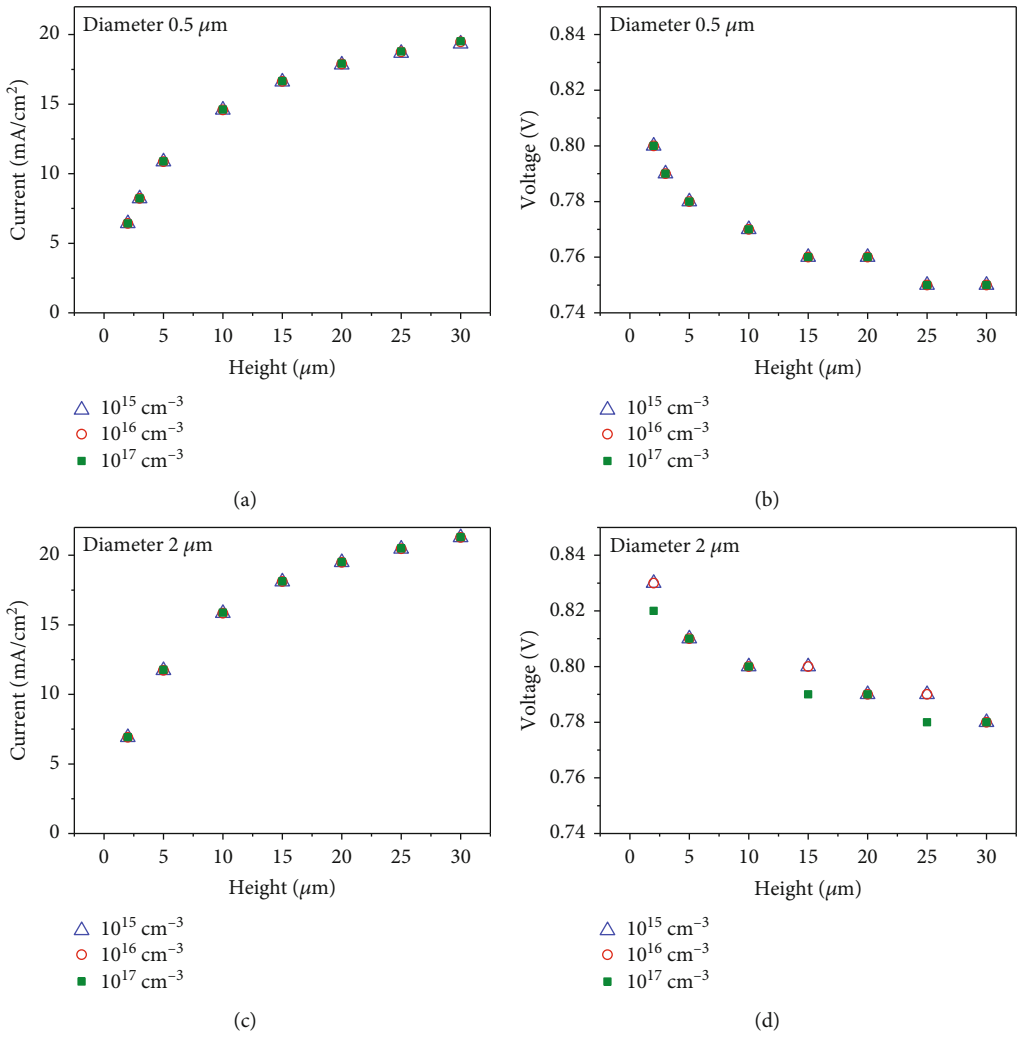

FIGURE 4: Calculated values of (a, c) J_{SC} and (b, d) V_{OC} for the bottom junction as a function of the height of silicon wires for the wire diameter of (a, b) 0.5 μm and (c, d) 2 μm and the MCC lifetime of 1 ms.

the space charge region overlaps, and practically, the entire volume of the wire becomes inverted. Complete inversion of the conductivity type in the Si wire is shown in Figure 6, which illustrates the calculated equilibrium band diagrams in sections along and across a Si wire with a diameter of 1 μm and doping of 10^{15} cm^{-3}. It can be seen that the electron concentration in the (n) c-Si wire approaches its equilibrium value only at the bottom of the wire at the interface with the (n)a-Si:H back contact. With an increase in the doping level, the width of the space charge region decreases. For 10^{17} cm^{-3}, it is about 0.1 μm, and for 0.5 μm, the wire will not be completely inverted. In this case, a higher V_{OC} value is observed (Figure 6) as opposed to a doping level of $\leq 10^{16}$ cm^{-3} when the wire is completely inverted. The effect of complete inversion of the wire is also less pronounced with an increase in its diameter. For doping of 10^{16} cm^{-3}, when the width of the space-charge region is about 0.3 μm at a wire diameter of 1 μm, complete inversion no longer occurs, which leads to a higher value of V_{OC} compared to doping of 10^{15} cm^{-3}.

The effect of complete inversion of the Si wire has a much stronger effect on the performance of the SC in the case of lower MCC lifetimes, since in the absence of a pulling field in the wire, the transport of carriers is determined only by diffusion, and the level of recombination will be significantly higher in comparison with higher lifetimes. This effect even leads to a decrease in J_{SC} with an increase in the wire height for a diameter of 0.5 μm and a doping level of 10^{15} cm^{-3}.

However, even though for higher minority-carrier lifetimes, the effect of complete inversion of wires does not affect so significantly the performance of the bottom junction; in a real situation, it cannot be neglected when using Si with a high carrier lifetime. It should be noted that a simplified model was used in the calculation, which does not take into account any surface states at the a-Si:H/c-Si interface. In practice, in the case of complete inversion, the surface states presenting at this boundary will lead to a strong decrease in the conversion efficiency. The fact is that in the absence of an electric field that prevents the flow of electrons to the interface the surface states will make a more significant contribution to recombination losses, as was experimentally shown in [18].

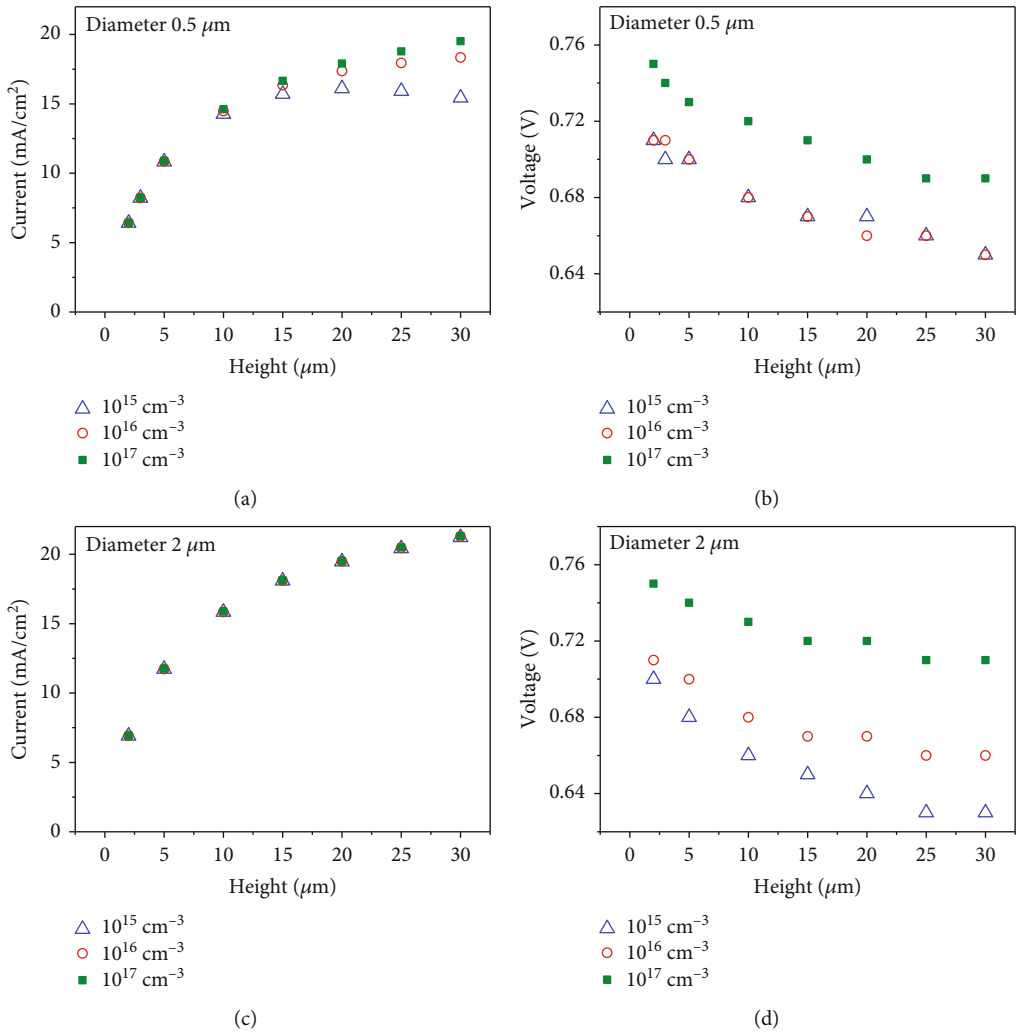

Figure 5: Calculated values of (a, c) J_{SC} and (b, d) V_{OC} for the bottom junction as a function of the height of silicon wires for a wire diameter of (a, b) 0.5 μm and (c, d) 2 μm and the MCC lifetime in (n) c-Si 10 μs.

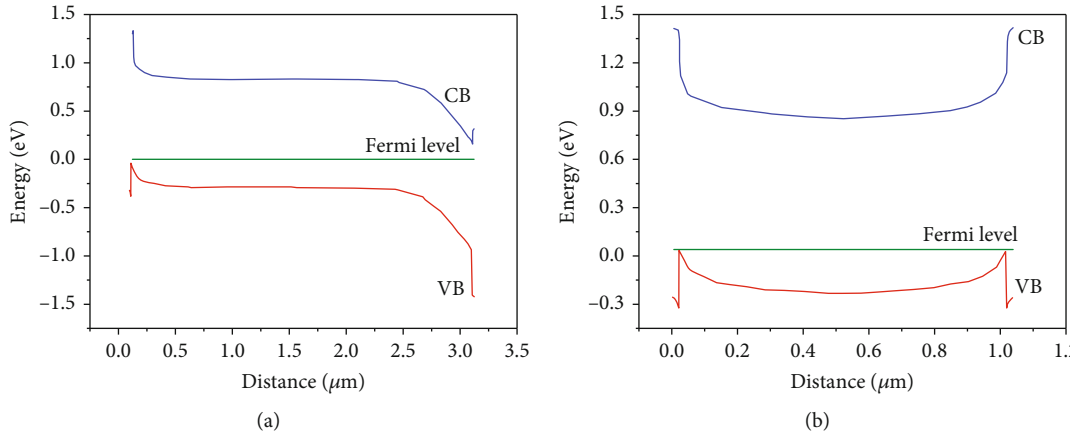

Figure 6: Energy band diagrams under equilibrium conditions obtained (a) along (from top to bottom) the wire and (b) the second for the case across the wire with a length of 3 μm, a diameter of 1 μm, and doping of 1015 sm^{-3}.

3.2. Top Junction. The performance calculation for the top junction based on the a-Si:H p-i-n structure showed that an increase in the wire height leads to an increase in J_{SC} because the length of the light absorption region increases. At a wire height of more than 15 μm, there is a tendency for J_{SC} to saturate; an insignificant J_{SC} increase is observed.

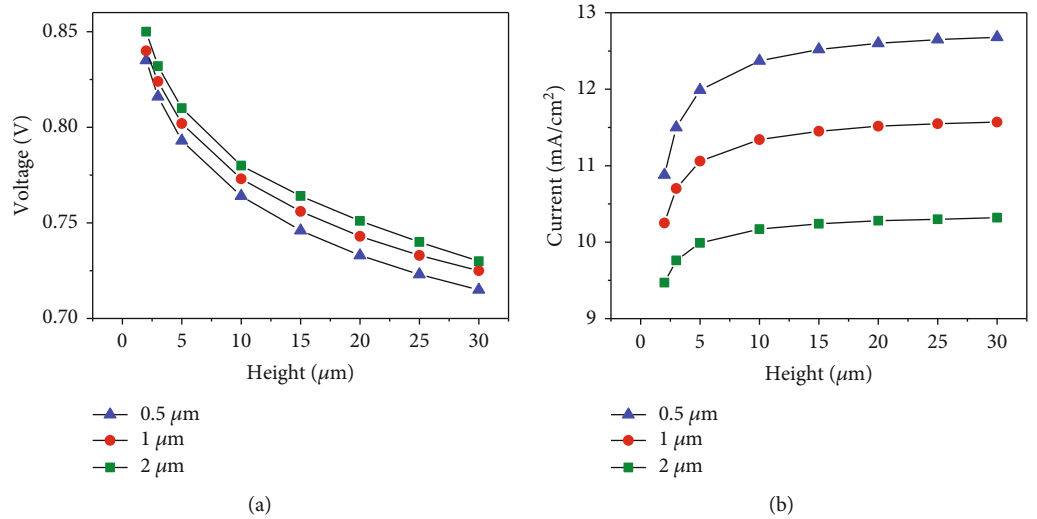

FIGURE 7: Calculated values of (a) V_{OC} and (b) J_{SC} for the top junction created on the wire of various diameters and heights.

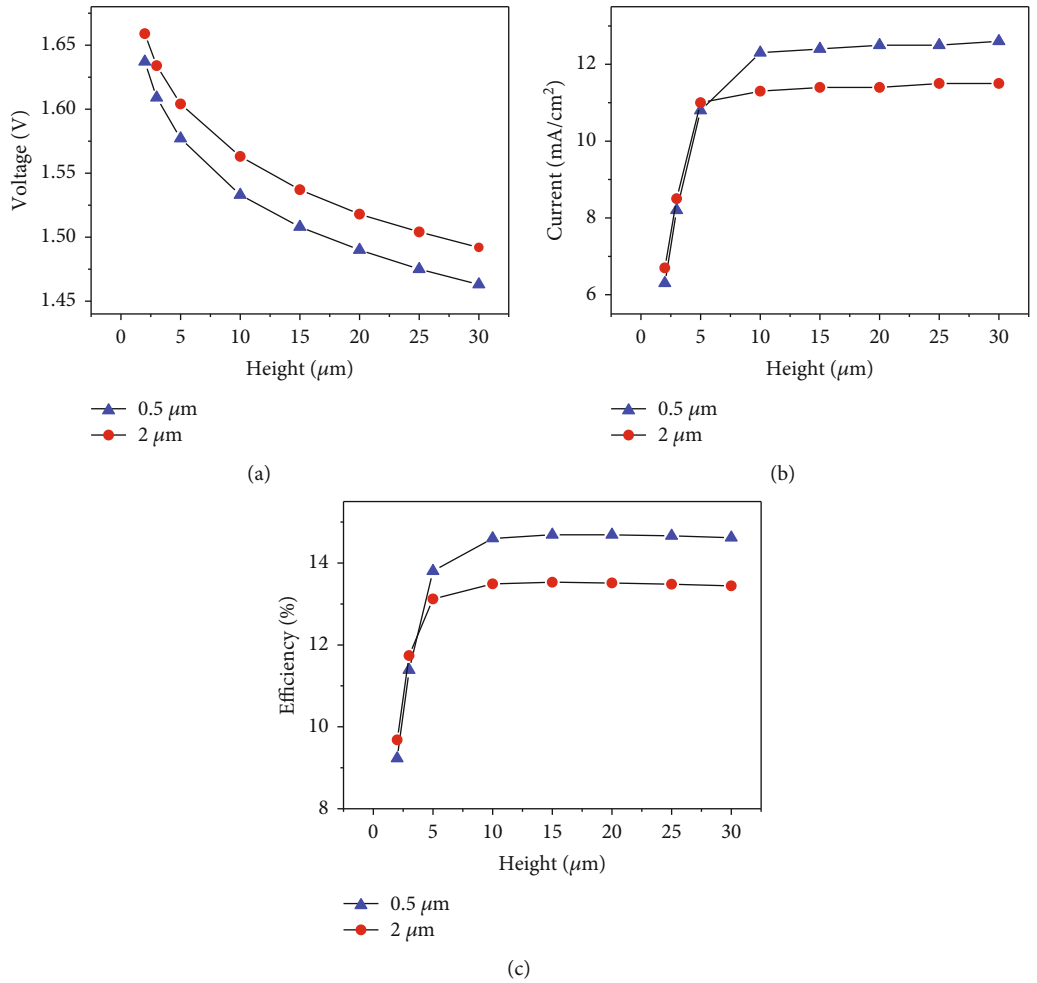

FIGURE 8: Dependences of (a) V_{OC}, (b) J_{SC}, and the (c) efficiency on the height of the Si wire for the MCC lifetime of 1 ms and the wire diameter of 0.5 μm and 2 μm.

However, in this case, a decrease in V_{OC} is also observed due to the nonuniform distribution of the absorbed light and, consequently, the concentration of nonequilibrium charge carriers. Closer to the wire bottom, the concentration of non-equilibrium charge carriers is lower, which leads to a decrease in the generated V_{OC} in this region and, consequently, in the

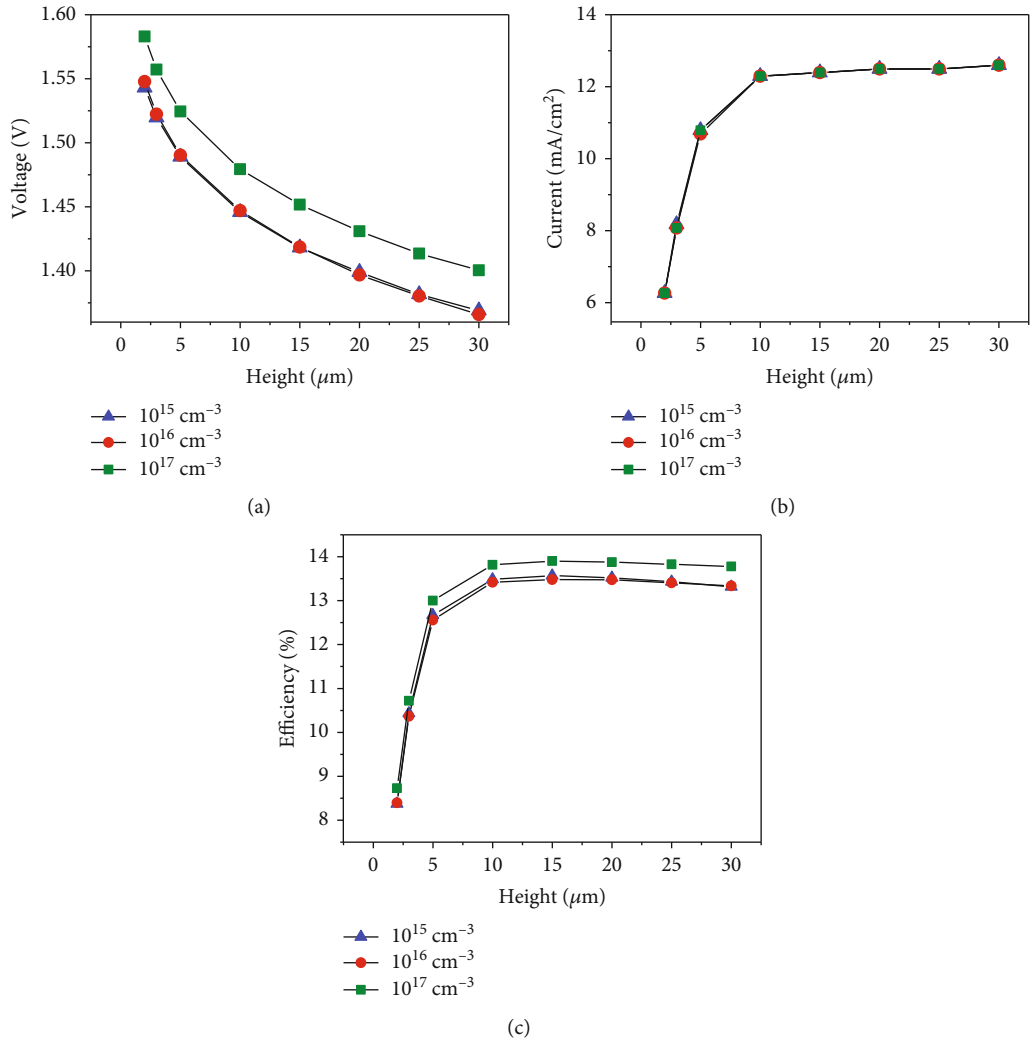

FIGURE 9: Dependences of (a) V_{OC}, (b) J_{SC}, and the (c) efficiency on the height of the Si wire for different doping levels; the MCC lifetime is 10 μs, and the wire diameter is 0.5 μm.

entire SC due to the equipotentiality of the contact layers. In practice, this effect should be less pronounced, because the calculation used the vertical path of the rays and did not take into account their deviation from the vertical, as well as possible diffuse scattering in the polymer matrix, which should lead to a more uniform distribution of nonequilibrium charge carriers.

The absolute value of J_{SC} strongly depends on the diameter of the Si wire. With a decrease in the diameter of the Si wire, the contribution of the area of the vertical section of the *i*-layer of the top p-i-n junction to the total area of the SC becomes larger, which leads to an increase in J_{SC} of the top junction (Figure 7).

3.3. Tandem Solar Cell. Based on the results of separate junction simulations, a tandem SC was calculated. The J_{SC} value for the bottom junction based on Si wires is higher compared to that for the top junction. Thus, to approximate the current matching condition, the tandem SC was calculated based on vertically aligned structures with a diameter of 0.5 μm, for which the maximum J_{SC} value was reached (Figures 8 and 9). The V_{OC} value decreases monotonically with an increase in the height of the Si wires, while J_{SC} limited by the top junction sharply increases with an increase in the height to 10 μm, and then, it weakly depends on the height of the wires. This behavior determines the presence of a maximum in the dependence of the efficiency of the tandem SC on the height of the Si wire, which is in the range of 10-15 μm. The maximum values of the efficiency for an MCC lifetime of 1 ms do not exceed 15%. However, the most interesting result is that the efficiency for structures based on Si wires with a lifetime of 10 μs reaches 14%. This result demonstrates the promises of the proposed approach since it opens up the possibility of creating flexible SCs based on Si wires of 10 μm in height with an MCC lifetime of tens of μs having an efficiency at the level of industrially produced SCs based on wafers (300 μm) of crystalline and polycrystalline silicon (14-16%).

The possibility of practical implication of the proposed tandem structure design was explored. First, a way to form the Si wire array was chosen.The vapor-liquid-solid method (VLS) is commonly used for Si nanowire growth [19, 20].

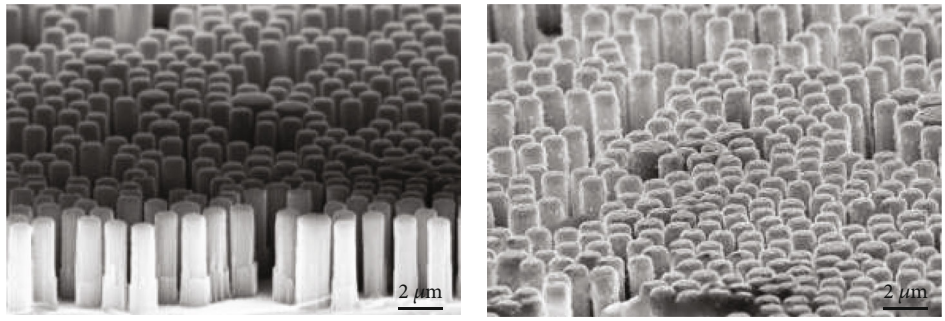

(a) (b)

Figure 10: SEM 20° tilt images of a-Si:H/c-Si vertical-aligned tandem test structure before (a) and after (b) top ITO layer deposition.

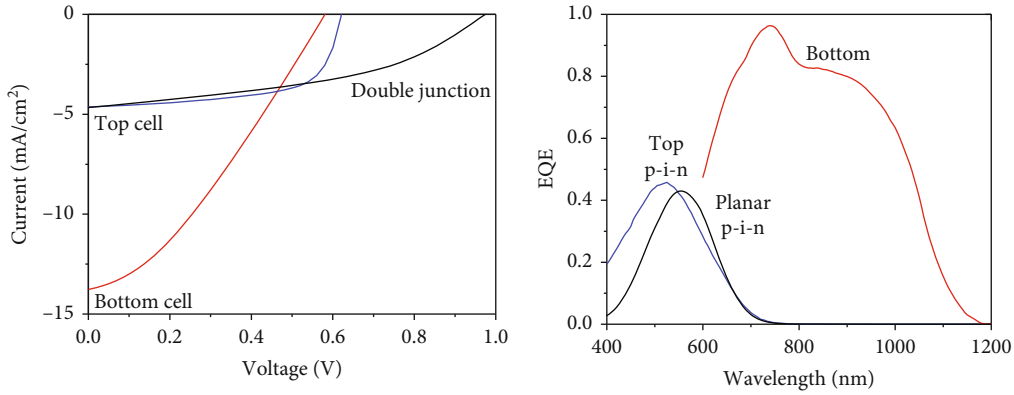

(a) (b)

Figure 11: Experimental I-V curves (a) and EQE spectra (b) for the tandem a-Si:H/c-Si test solar cell structure.

However, the diameter of Si wires obtained by this technique is normally limited by 0.1-0.2 μm being out of the required range. The same limitation does not allow one to use another well-known method for the formation of Si wires, namely, metal-assisted catalytic etching (MACE) [21, 22]. The required Si wire diameter and height could be archived by dry plasma etching at cryogenic temperatures [23]. This technology was successfully adopted for photovoltaic applications using latex sphere lithography with an intermediate step of SiO_2 hard mask formation [24]. The latex sphere lithography approach allows one to avoid the time-consuming photolithography process. The application of SiO_2 hard mask provides the way to form Si wire height exceeding 1 μm. Single junction core-shell a-Si:H/c-Si heterojunction solar cells based on an array of periodic Si wires were fabricated by this technique [18]. A relatively low value of V_{OC} (0.5 V) was obtained because of nonoptimized a-Si:H/c-Si interface passivation, which requires further a-Si:H deposition process development. However, similar structures may be used as a bottom junction to check the feasibility of tandem solar cell fabrication. Here, the tandem solar cell based on vertically aligned Si structures was formed. The Si wires with a height of 4 μm and diameter of 1.5 μm were fabricated by cryogenic plasma etching using latex sphere lithography and SiO_2 hard mask as described elsewhere [24]. N-type Si substrate with a doping level of 2×10^{15} was used. To form the bottom (p)a-Si:H/(n)c-Si heterojunction, the layers of a-Si:H were deposited by plasma-enhanced chemical vapor deposition (PECVD). A thin (3-5 nm) layer of undoped a-Si:H was deposited to passivate the Si surface, followed by 20 nm of p-type doped a-Si:H layer. Then, the surface of the bottom junction was covered by a 100 nm thick ITO layer using magnetron sputtering [18]. The ITO layer was used for electrical connection between the bottom and top junctions. A p-i-n structure based on a-Si:H ((p)20 nm/(i)200 nm/(n)20 nm) was deposited on the ITO by PECVD under similar conditions described in [8]. On the backside of the Si substrate, a 20 nm thick n-type phosphorus-doped a-Si:H layer was deposited. Finally, an ITO layer was sputtered on the front side of the a-Si:H/c-Si tandem structure to form the top electrode. Silver paste and vacuum evaporated Ag layer were used for the top and the bottom contacts, respectively. Scanning electron microscopy (SEM) images of the solar cells before and after top ITO deposition are presented in Figures 10(a) and 10(b), respectively. The top ITO layer fully covers the vertically aligned tandem structures.

The I–V curves measured under AM1.5G (100 mW/cm^2) for the top and bottom junctions as well as the whole tandem solar cell are presented in Figure 11(a). The J_{SC} of the tandem cell is limited by that of the top junction. The absolute value of J_{SC} is about 30-40% lower compared to the simulation results because the top p-i-n junction exhibits quite low external quantum efficiency (EQE) (Figure 11(b)).

However, we should stress that it is due to the nonoptimized p-i-n structure design or deposition conditions. The EQE spectrum of the planar p-i-n structure is lower compared to that of the vertical-aligned p-i-n junction. Similarly, low V_{OC} values obtained for p-i-n structures (0.66 V for planar and 0.62 V for vertically aligned one) demonstrate their low quality. In contrast, significantly higher J_{SC} for the bottom junction compared to the simulation is caused by the contribution of the Si substrate, which was not taken into account in the simulation. Thus, an optimization of p-i-n structure and variation of the Si wire geometry (height and diameter) should be carried out for the quantitative analysis of the simulation results. However, the fabrication feasibility of the proposed tandem solar cell design was demonstrated.

4. Conclusions

The tandem SC performance calculation for an SC based on Si wires and p-i-n a-Si:H structures was carried out. The range of optimal values for the diameter and height of Si wires, as well as the level of their doping, has been determined. It was shown that it is possible to create flexible SCs of 10 μm thick, obtained using inexpensive silicon with a lifetime of 10 μs at an efficiency of 14%. The feasibility of tandem solar cell fabrication was experimentally demonstrated.

Data Availability

The simulation data used to support the findings of this study are available from the corresponding author upon request.

Conflicts of Interest

The authors state no conflict of interest.

Acknowledgments

The research was carried out within the framework of the project № FSEE-2020-0008, which was carried out within the framework № 075-01024-21-00 of the state assignment of Ministry of Science and Higher Education of the Russian Federation.

References

[1] B. Burger, "Electricity Generation in Germany in the First Half of 2021," vol. 6, Fraunhofer Institute for Solar Energy Systems ISE, Germany, Freiburg, 2021.

[2] M. A. Green, E. D. Dunlop, J. Hohl-Ebinger, M. Yoshita, N. Kopidakis, and X. Hao, "Solar cell efficiency tables (version 58)," *Progress in Photovoltaics*, vol. 29, no. 7, pp. 657–667, 2021.

[3] A. Richter, M. Hermle, and S. W. Glunz, "Reassessment of the limiting efficiency for crystalline silicon solar cells," *IEEE Journal of Photovoltaics*, vol. 3, no. 4, pp. 1184–1191, 2013.

[4] A. Augusto, E. Looney, C. del Cañizo, S. G. Bowden, and T. Buonassisi, "Thin silicon solar cells: pathway to cost-effective and defect-tolerant cell design," *Energy Procedia*, vol. 124, pp. 706–711, 2017.

[5] Y. Han, S. Meyer, Y. Dkhissi et al., "Degradation observations of encapsulated planar CH3NH3PbI3perovskite solar cells at high temperatures and humidity," *Journal of Materials Chemistry A*, vol. 3, no. 15, pp. 8139–8147, 2015.

[6] WIP Wirtschaft und Infrastruktur GmbH & Company Planungs-KG, *31st European Photovoltaic Solar Energy Conference and Exhibition: EU PVSEC 2015*, WIP Wirtschaft und Infrastruktur GmbH & Company Planungs-KG, Hamburg, Germany, 2015.

[7] E. Marins, M. Warzecha, S. Michard et al., "Flexible n-i-p thin film silicon solar cells on polyimide foils with textured ZnO:Ga back reflector," *Thin Solid Films*, vol. 571, pp. 9–12, 2014.

[8] A. S. Gudovskikh, I. A. Morozov, D. A. Kudryashov, E. V. Nikitina, and V. Sivakov, "Multijunction a-Si:H/c-Si solar cells with vertically-aligned architecture based on silicon nanowires," *Materials Today: Proceedings*, vol. 4, no. 7, pp. 6797–6803, 2017.

[9] O. V. Pylypova, A. A. Evtukh, P. V. Parfenyuk et al., "Electrical and optical properties of nanowires based solar cell with radial p-n junction," *Opto-Electronics Review*, vol. 27, no. 2, pp. 143–148, 2019.

[10] R. Vismara, O. Isabella, A. Ingenito, F. T. Si, and M. Zeman, "Geometrical optimisation of core-shell nanowire arrays for enhanced absorption in thin crystalline silicon heterojunction solar cells," *Beilstein Journal of Nanotechnology*, vol. 10, pp. 322–331, 2019.

[11] M. Zanuccoli, J. Michallon, I. Semenihin et al., "Numerical simulation of vertical silicon nanowires based heterojunction solar cells," *Energy Procedia*, vol. 38, pp. 216–222, 2013.

[12] L. Huang and J. Povinelli, "Limiting efficiencies of tandem solar cells consisting of III-V nanowire arrays on silicon," *Journal of Applied Physics*, vol. 112, no. 6, article 064321, 2012.

[13] S. Abdellatif and K. Kirah, "Numerical modeling and simulation for a radial p-i-n nanowire photovoltaic device," *Energy Procedia*, vol. 36, pp. 488–491, 2013.

[14] D. Diouf, I. Ngo, J.-P. Kleider, M. Gueunier-Farret, and J. Alvarez, "Nanowire solar cells using hydrogenated amorphous silicon: a modeling study," *Physica Status Solidi*, vol. 209, no. 6, pp. 1026–1030, 2012.

[15] K. Miyazaki, N. Matsuki, H. Shinno, H. Fujioka, M. Oshima, and H. Koinuma, "Device simulation and fabrication of field effect solar cells," *Bulletin of Materials Science*, vol. 22, no. 3, pp. 729–733, 1999.

[16] S. Michael, A. D. Bates, and M. S. Green, "Silvaco ATLAS as a solar cell modeling tool," in *Conference Record of the Thirty-first IEEE Photovoltaic Specialists Conference*, vol. 2005, pp. 719–721, Lake Buena Vista, FL, USA, 2005.

[17] A. S. Gudovskikh, A. S. Abramov, A. V. Bobyl et al., "Study of the properties of solar cells based on a-Si:H p-i-n structures by admittance spectroscopy," *Semiconductors*, vol. 47, no. 8, pp. 1090–1096, 2013.

[18] A. S. Gudovskikh, D. Kudryashov, A. Baranov et al., "Impact of interface recombination on quantum efficiency of a-Si:H/c-Si solar cells based on Si wires," *Physica Status Solidi*, vol. 218, no. 22, article 2100339, 2021.

[19] J. Westwater, "Growth of Silicon Nanowires via Gold/Silane Vapor–Liquid–Solid Reaction," in *Journal of Vacuum Science & Technology B*, vol. 15, no. 3p. 554, Struct, 1997.

[20] Y. Wang, V. Schmidt, S. Senz, and U. Gösele, "Epitaxial growth of silicon nanowires using an aluminium catalyst," *Nature Nanotechnology*, vol. 1, no. 3, pp. 186–189, 2006.

[21] V. Sivakov, G. Andrä, A. Gawlik et al., "Silicon nanowire-based solar cells on glass: synthesis, optical properties, and cell parameters," *Nano Letters*, vol. 9, no. 4, pp. 1549–1554, 2009.

[22] Z. Huang, N. Geyer, P. Werner, J. de Boor, and U. Gösele, "Metal-assisted chemical etching of silicon: a review," *Maternité*, vol. 23, no. 2, pp. 285–308, 2011.

[23] R. Dussart, T. Tillocher, P. Lefaucheux, and M. Boufnichel, "Plasma cryogenic etching of silicon: from the early days to today's advanced technologies," *Journal of Physics D: Applied Physics*, vol. 47, no. 12, article 123001, 2014.

[24] I. Morozov, A. Gudovskikh, A. Uvarov, A. Baranov, V. Sivakov, and D. Kudryashov, "The Study of Latex Sphere Lithography for High Aspect Ratio Dry Silicon Etching," *Physica Status Solidi A*, vol. 217, article 1900535, 2019.